An Investigation of the High-Temperature and Solidification Microstructures of PH 13-8 Mo Stainless Steel

M.J. CIESLAK, C.R. HILLS, P.F. HLAVA, and S.A. DAVID

Differential thermal analysis (DTA), high-temperature water-quench (WQ) experiments, and optical and electron microscopy were used to establish the near-solidus and solidification microstructures in PH 13-8 Mo. On heating at a rate of 0.33 °C/s, this alloy begins to transform from austenite to δ-ferrite at ≈1350 °C. Transformation is complete by ≈1435 °C. The solidus is reached at ≈1447 °C, and the liquidus is ≈1493 °C. On cooling from the liquid state at a rate of 0.33 °C/s, solidification is completed as δ-ferrite with subsequent transformation to austenite beginning in the solid state at ≈1364 °C. Insufficient time at temperature is available for complete transformation and the resulting room-temperature microstructure consists of matrix martensite (derived from the shear decomposition of the austenite) and residual δ-ferrite. The residual δ-ferrite in the DTA sample is enriched in Cr (≈16 wt pct), Mo (≈4 wt pct), and Al (≈1.5 wt pct) and depleted in Ni (≈4 wt pct) relative to the martensite (≈12.5 wt pct Cr, ≈2 wt pct Mo, ≈1 wt pct Al, ≈9 wt pct Ni). Solid-state transformation of $\delta \Rightarrow \gamma$ was found to be quench-rate sensitive with large grain, fully ferritic microstructures undergoing a massive transformation as a result of water quenching, while a diffusionally controlled Widmanstätten structure was produced in air-cooled samples.

I. INTRODUCTION

PH 13-8 Mo is a precipitation hardenable martensitic stainless steel (Fe-13Cr-8Ni-2Mo-1Al wt pct) which can, in the wrought condition, achieve a tensile yield strength in excess of 200 ksi.[1] Chemically balanced to effectively eliminate ferrite (δ) in the wrought condition and produced by double vacuum melting techniques, this alloy also has superior ductility and fracture toughness when compared to 17-4 PH and 15-5 PH stainless steels. Recent interest in this material as a casting alloy has driven the need to understand the development of microstructure in as-solidified product. The literature is virtually bereft of information concerning as-cast PH 13-8 Mo.[2] What little information exists relative to the solidification of this alloy concerns its weldability.[3,4,5]

The purpose of the present investigation, therefore, was to establish the phase relationships which occur during the melting and solidification of this alloy in order to allow for improved metallurgical interpretation of microstructures observed in cast and welded products. In doing so, this paper describes, through the analysis of microstructures quenched from high homologous temperatures and from interrupted solidification experiments, the evolution of microstructure as a result of solidification processing of PH 13-8 Mo.

M.J. CIESLAK, Supervisor, Physical Metallurgy Division, C.R. HILLS, Member of Technical Staff, and P.F. HLAVA, Senior Member of Technical Staff, Electron Optics and X-ray Analysis Division, are with Sandia National Laboratories, Albuquerque, NM 87185. S.A. DAVID, Group Leader, Materials Joining, is with the Metals and Ceramics Division, Oak Ridge National Laboratory, Oak Ridge, TN 37831.

Manuscript submitted December 13, 1989.

II. EXPERIMENTAL PROCEDURE

The composition of the PH 13-8 Mo stainless steel used in this study is given in Table I. The product form was rectangular bar stock (Condition A—solution annealed) approximately 25 by 6 mm in cross section. The martensitic microstructure of the as-received bar stock is shown in Figure 1. From this material, samples were prepared for both differential thermal analysis (DTA) and high-temperature water-quench (WQ) experiments. Rectangular samples 5 g or less in weight were used for both the DTA and WQ experiments.

Differential thermal analysis experiments were performed using a Netsch STA 429 Thermal Analyzer. Tungsten was the reference material. Both the reference material and the PH 13-8 Mo samples were held in high-purity alumina crucibles during the DTA tests. All tests were run in a flowing He environment at heating and cooling rates of 0.33 °C/s. The peak temperature during testing was 1550 °C. All tests were terminated at 1000 °C and then furnace cooled to room temperature.

The WQ tests were performed in a vertical Astro Model 1000 alumina tube furnace with graphite heating elements equipped with a waterdrop-quenching chamber. Samples were held in the hot zone in high-purity alumina crucibles which were, in turn, suspended by a refractory metal wire. At the appropriate time during the test run, a valve below the furnace hot zone was opened and the sample/crucible/wire combination was dropped into a water-quench bath held at ≈10 °C. The Astro furnace was constructed such that the system could be evacuated and backfilled with an inert gas (Ar). A series of evacuations and backfillings was performed before starting the test, and during the running of the experiments, a flowing Ar atmosphere was maintained by opening a

Table I. Alloy Composition

Element	Concentration*
Cr	12.57
Ni	8.09
Mo	2.14
Al	1.18
C	0.026
Mn	0.01
Si	0.02
P	<0.005
S	0.004
N	0.002

*All values in weight percent, balance iron.

small vent valve on the exit line. All tests involved heating and cooling at a rate of 0.33 °C/s to be consistent with the DTA experiments. Samples quenched during the heating portion of the cycle (below the melting temperature) were held at the indicated temperature for typically 4 minutes in order to establish equilibrium structures. Samples tested during the cooling portion of the cycle (subsequent to melting) were quenched immediately upon reaching the desired temperature.

Microstructural analysis began with optical metallography. Samples were mounted in BAKELITE* and polished through 0.05-μm alumina. Samples were etched using either Vilella's reagent or a 10 pct oxalic acid solution for times necessary (typically 10 to 30 seconds) to reveal the structure. Both bright-field and differential interference contrast (DIC) techniques were used. Differential interference contrast metallography was especially useful for discerning the martensite laths which developed during the shear transformation of the high-temperature austenite (γ) structure.

*BAKELITE is a trademark of Union Carbide Corporation, Danbury, CT.

Further analysis of the microstructures involved electron microprobe and transmission electron microscopy (TEM) techniques. A Cameca MBX microprobe and a JEOL Superprobe were used to quantify the elemental partitioning between and within the room-temperature phases. A $\Phi(\rho,Z)$[6] algorithm was used to convert the raw counting data into weight percentages. A JEOL 2000FX analytical electron microscope (AEM), operating at 200 kV accelerating potential and equipped with a TRACOR NORTHERN* TN2000 energy dispersive spectrometer (EDS), was used for the analysis of thin foils. Selected area electron diffraction was used to identify the phases present. Martensite was readily differentiated from δ based upon both chemical composition and the much higher dislocation density in the martensite laths.

*TRACOR NORTHERN is a trademark of Tracor Northern, Inc., Middleton, WI.

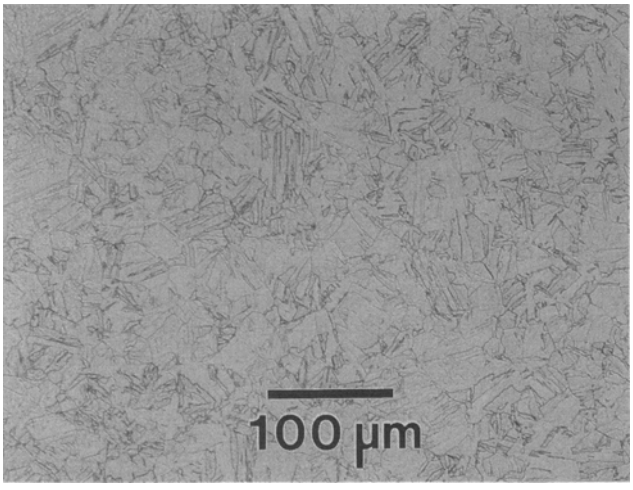

Fig. 1—Martensitic microstructure of as-received PH 13-8 Mo.

III. RESULTS

A. *DTA Sample*

Figure 2 shows a DTA thermogram obtained from PH 13-8 Mo. The lower temperature responses have been eliminated in order to focus on the higher temperature transformations influencing the melting and solidification behavior. From the thermogram, it can be clearly seen that an endothermic reaction begins at ≈1350 °C on heating, peaks at ≈1411 °C, and terminates by ≈1440 °C. A second, much larger endothermic reaction begins at ≈1447 °C, peaks at ≈1493 °C, and terminates by ≈1518 °C. On cooling, a large exothermic reaction initiates at ≈1469 °C, peaks at ≈1445 °C, and terminates by ≈1411 °C. A smaller exothermic reaction begins at ≈1364 °C, peaks at ≈1351 °C, and terminates by ≈1324 °C.

The microstructure of the DTA sample is shown in the micrograph in Figure 3 and consists of two phases. The matrix phase (martensite, as described below) has a lath-like substructure. The minor phase (δ, as described below) appears featureless. An electron microprobe trace made on the DTA sample between the two hardness indentations seen in Figure 3 is presented in Figure 4. The minor phase is enriched in Cr (≈16 wt pct), Mo (≈4 wt pct), and Al (≈1.5 wt pct) and depleted in Ni (≈4 wt pct) as compared with the matrix phase (≈12.5 wt pct Cr, ≈2 wt pct Mo, ≈1 wt pct Al, ≈9 wt pct Ni).

B. *WQ Experiments*

Quenching temperatures during the thermal excursions were selected to analyze the microstructural evolution characterized by the observed endothermic and exothermic reactions during the DTA experiments.

1. *On-heating samples*

Figures 5 through 8 show the microstructures obtained from samples water quenched from 1300 °C, 1425 °C, 1435 °C, and 1448 °C, respectively. The microstructure seen in Figure 5, the sample water quenched from 1300 °C, is fully martensitic and, therefore, morphologically similar to that observed in the as-received product (Figure 1). It is clear that grain growth has occurred during the thermal excursion to 1300 °C resulting in a coarser martensite lath structure than that observed in the as-received product.

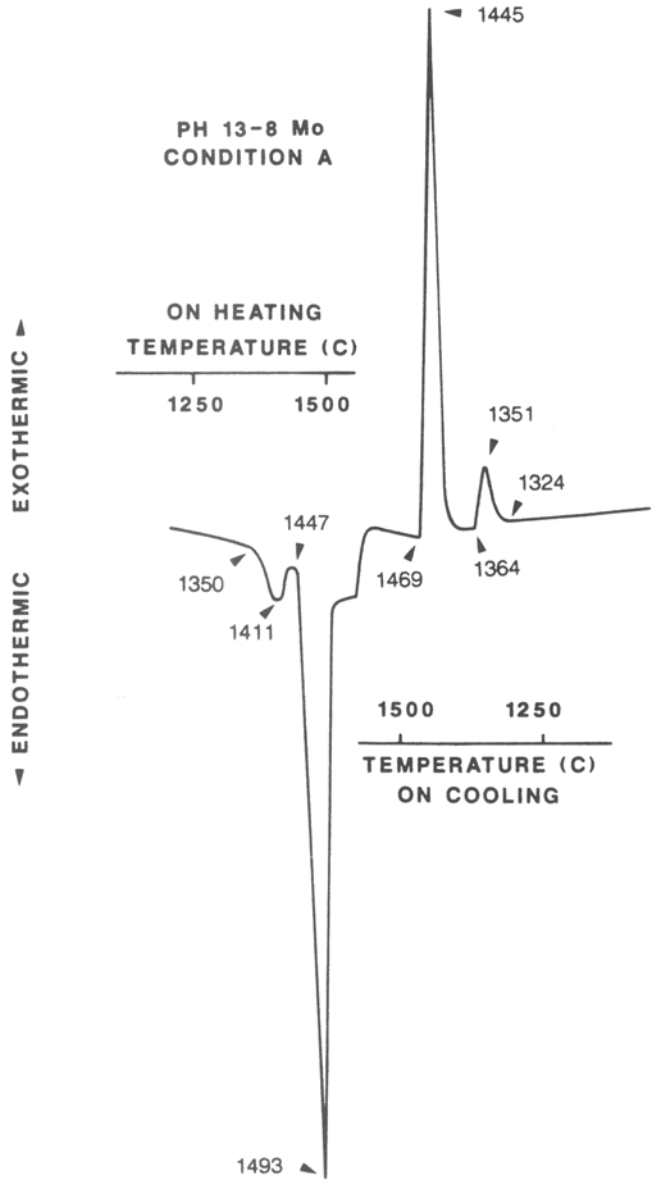

Fig. 2—DTA thermogram obtained from PH 13-8 Mo.

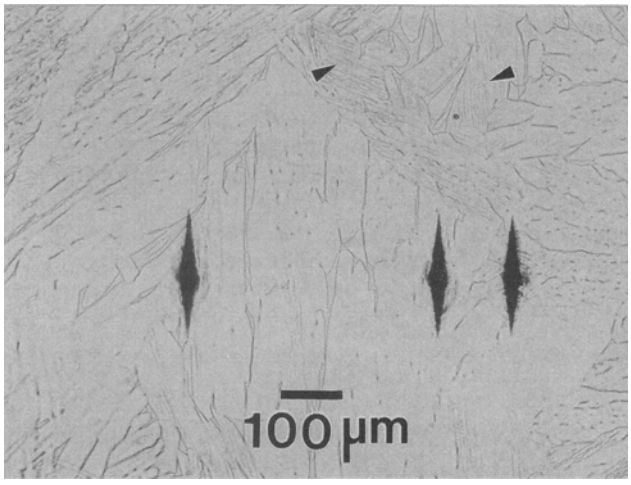

Fig. 3—Microstructure of DTA test sample of PH 13-8 Mo. Arrows identify martensite laths. Microhardness indentations bound position of microprobe trace shown in Fig. 4.

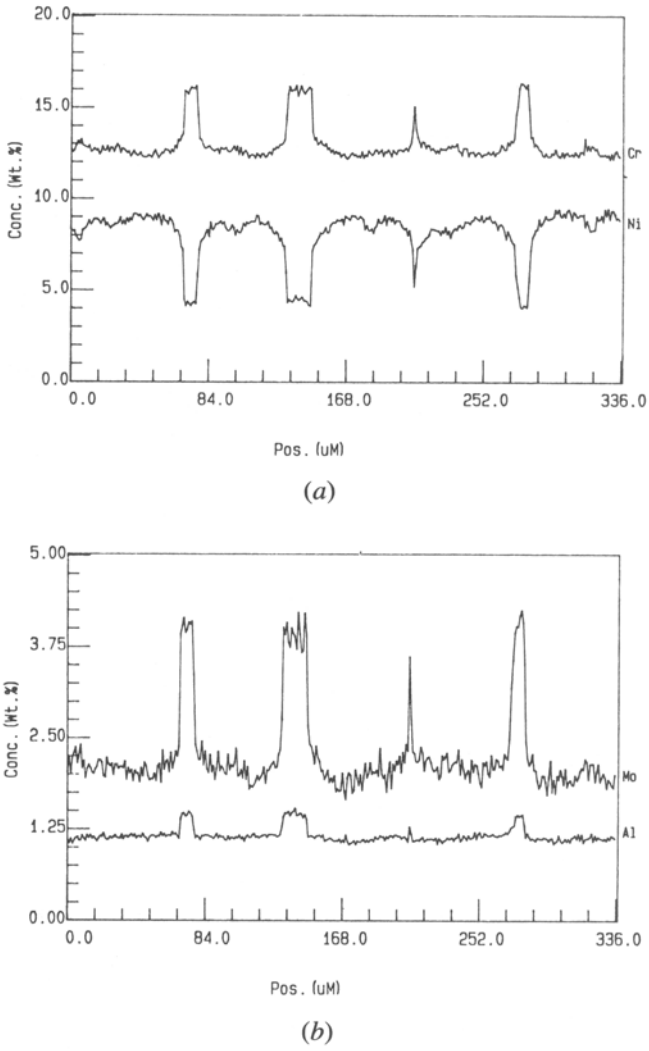

Fig. 4—Microprobe profiles taken on DTA test sample shown in Fig. 3: (*a*) Cr, Ni and (*b*) Mo, Al. Cameca MBX microprobe, 15 kV, 21 nA specimen current.

The microstructure observed in Figure 6, from the sample water quenched from 1425 °C, is quite different from that observed in either Figure 1 or 5. In addition to the light etching regions composed of a martensite lath substructure, a second microstructural constituent having a Widmanstätten-type morphology is also present. The presence of the Widmanstätten structure suggests that a breakdown of a higher temperature stable phase (δ) has occurred during quenching.

The microstructures observed in Figures 7 and 8, samples water quenched from 1435 °C and 1448 °C, respectively, contained very large grains. In contrast to the microstructure shown in Figure 6, a pronounced Widmanstätten structure, resulting in the retention of relatively large amounts of the high-temperature phase (δ), was not observed. Instead, the substructure appeared to be entirely martensitic (Figures 7 and 8(b)) with only occasional grain boundary structure observed in the 1448 °C sample (Figure 8(c)). Areas of incipient melting were also observed along some grain boundaries and at isolated areas within the grains (arrows in Figure 8(a)) in the

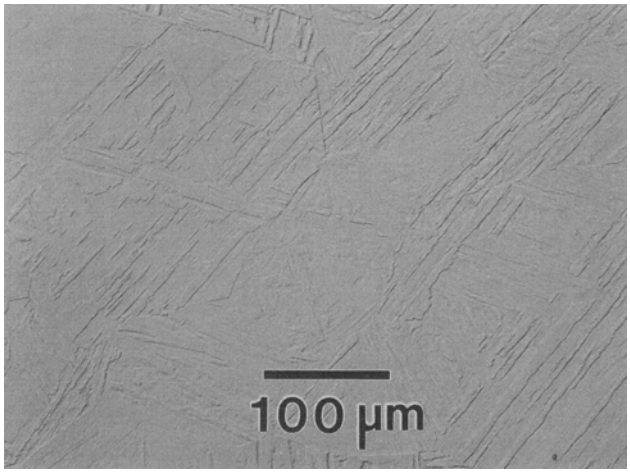

Fig. 5—Microstructure of 1300 °C (on-heating, water-quench) sample.

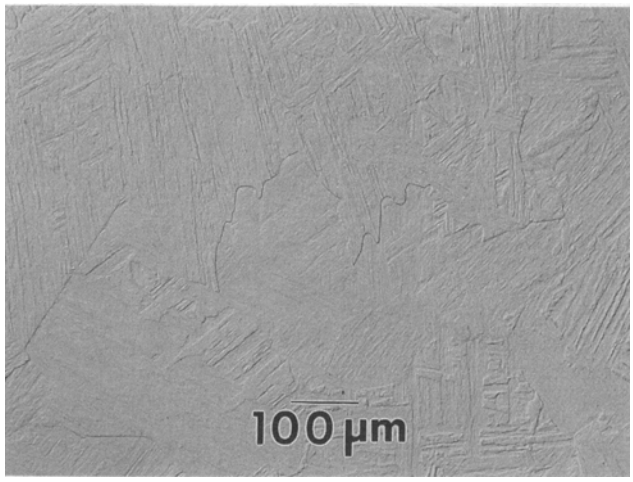

Fig. 7—Microstructure of 1435 °C (on-heating, water-quench) sample showing fully martensitic structure.

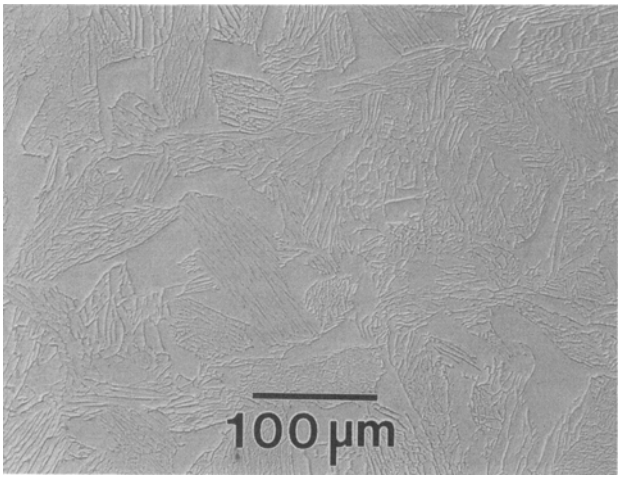

(*a*)

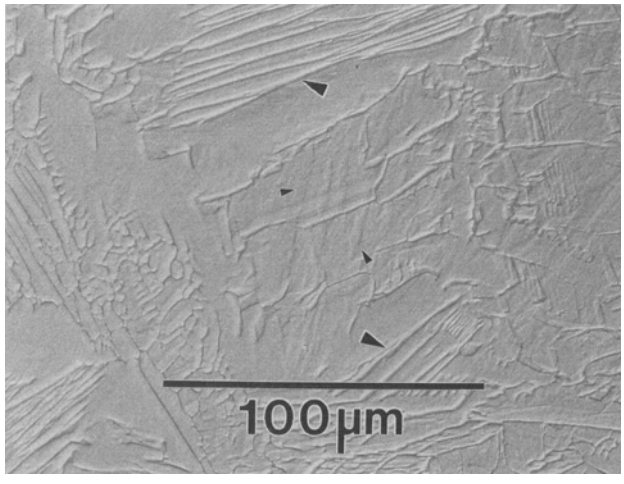

(*b*)

Fig. 6—(*a*) Microstructure of 1425 °C (on-heating, water-quench) sample. (*b*) Higher magnification image showing Widmanstätten (large arrows) and martensite lath (small arrows) substructures.

1448 °C sample, confirming that the alloy solidus had been reached during this thermal treatment. (The microhardness indentations in Figure 8(a) bracket regions for electron microprobe analysis, as will be discussed below.)

2. *On-cooling samples*

Figures 9 through 11 show the microstructures obtained from samples water quenched after melting the alloy (thermal excursion to a peak temperature of 1550 °C). Figure 9 shows the microstructure obtained as a result of water quenching a sample from 1450 °C. A cellular solidification structure can be observed. It is also clear that solidification has not proceeded to completion, as there are intercellular regions in which a much finer solidification substructure is observed, likely forming as a result of the rapid cooling encountered during the water quench. Within the cellular structure can be seen a Widmanstätten substructure similar to that observed in the specimen quenched from 1425 °C on heating, again suggesting a decomposition of the high-temperature δ phase during the quenching operation.

Figure 10 shows the microstructure of the sample quenched from 1375 °C on cooling. No evidence remains of the solidification event, except for the presence of shrinkage cavities, suggesting that some degree of homogenization occurred below the solidus temperature. The microstructure consists of coarse Widmanstätten-type features and large areas of single-phase martensite.

Figure 11 shows the microstructure of the sample quenched from 1300 °C. A two-phase microstructure is observed, consisting of a featureless minor constituent in a matrix containing a lath substructure. This microstructure is essentially identical to that observed in the DTA sample (Figure 3).

IV. ANALYSIS AND DISCUSSION

A. *Microstructural Development on Heating*

Interpretation of elevated-temperature microstructures in martensitic steels is often difficult because of the

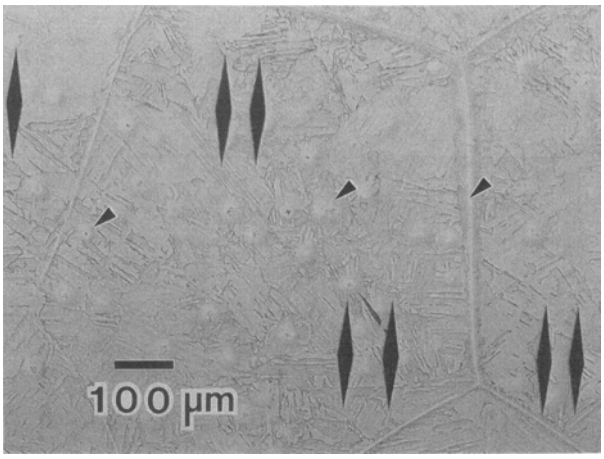

(*a*)

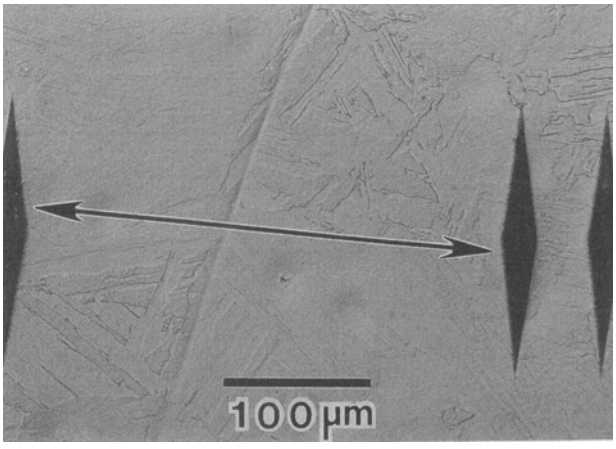

(*b*)

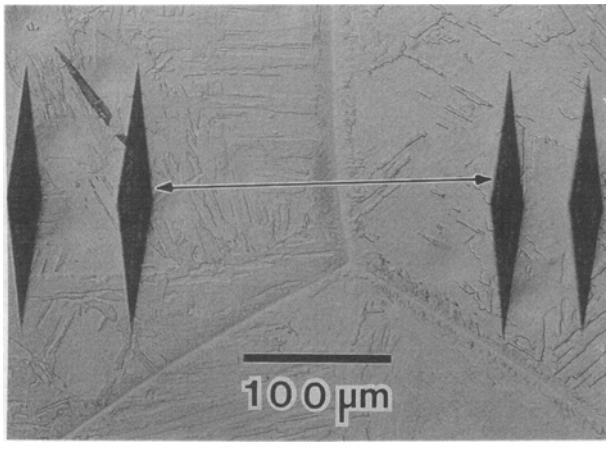

(*c*)

Fig. 8—(*a*) Microstructure of 1448 °C (on-heating, water-quench) sample; arrows indicate regions of incipient melting (note martensitic lath structure). (*b*) Higher magnification image of prior δ/δ grain boundary near the surface of the sample (note complete martensite lath structure). (*c*) Higher magnification image of prior δ/δ grain boundary more interior to the sample (note grain boundary structure and martensite lath substructure internal to the grains). Arrows indicate positions of microprobe traces shown in Figs. 15(b) and (c).

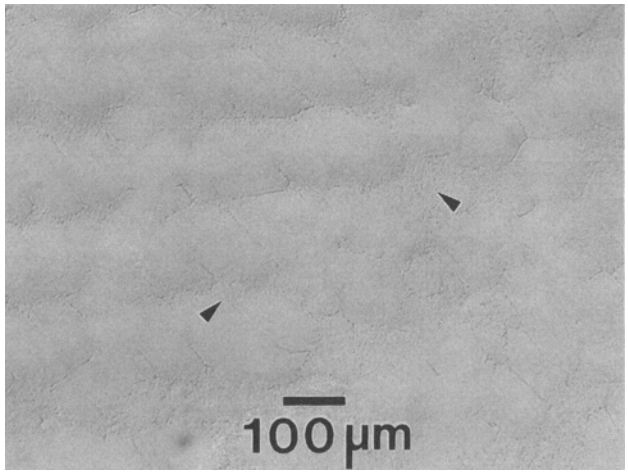

(*a*)

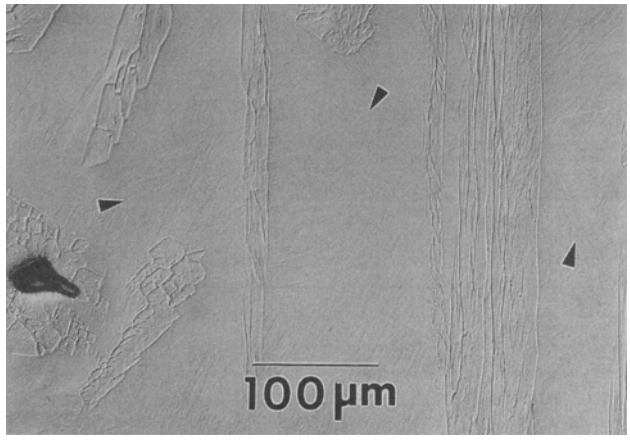

(*b*)

Fig. 9—(*a*) Cellular solidification microstructure of 1450 °C (on-cooling, water-quench) sample; arrows indicate intercellular regions which were liquid at the time of quenching. (*b*) Higher magnification image showing Widmanstätten substructure within the solidification cells.

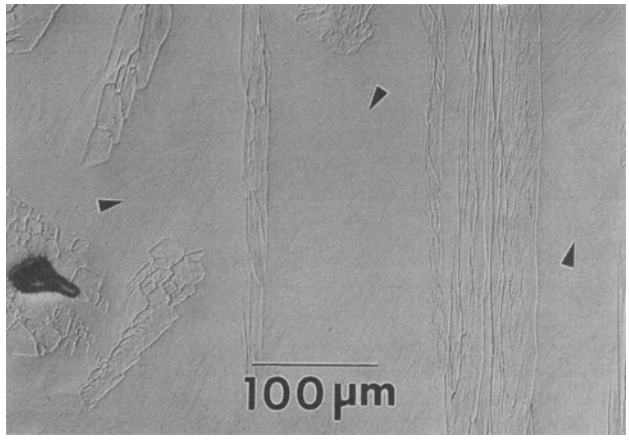

Fig. 10—Microstructure of 1375 °C (on-cooling, water-quench) sample showing a coarse Widmanstätten structure and large regions of single-phase martensite (arrows). Note no appearance of a remnant solidification structure.

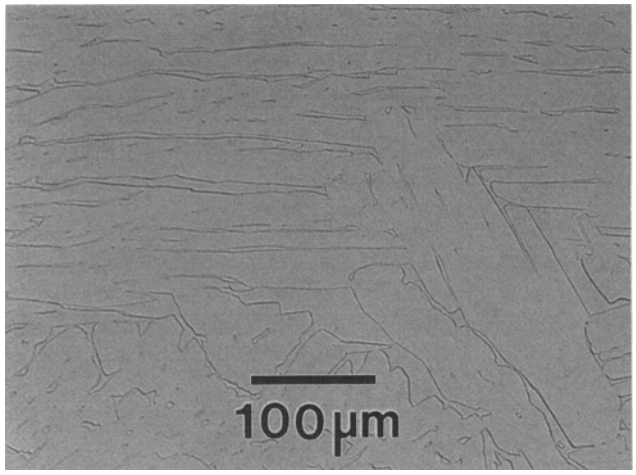

Fig. 11—Microstructure of 1300 °C (on-cooling, water-quench) sample.

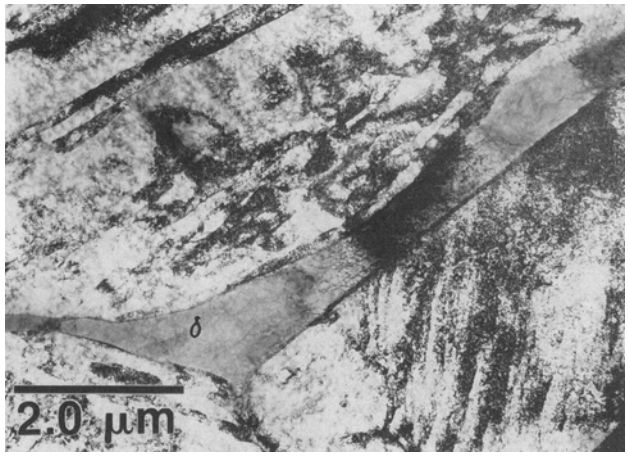

Fig. 12—TEM thin foil micrograph showing the two-phase δ + martensite microstructure seen in Fig. 6.

metastable nature of the parent γ phase. In the case of PH 13-8 Mo, a further complication arises because of the near-solidus transformation of γ to δ, as will be described below.

From the literature,[1] the martensite ⇒ γ reversion temperature is approximately 800 °C. It is clear from both the optical metallography and the DTA results of this study that γ is the stable phase in PH 13-8 Mo until ≈1350 °C. That is, quenched samples display fully martensitic microstructures, implying single-phase γ stability prior to quenching. Above that temperature, the microstructure is not stable as a single phase. Transmission electron microscopy analysis (selected area electron diffraction) of the sample quenched from 1425 °C on heating revealed a two-phase microstructure of δ and martensite. An orientation relationship, $[110]_\delta // [111]_{Mart}$:$(110)_\delta // (110)_{Mart}$, was commonly observed between the two phases. No retained γ was observed. Figures 12 and 13 show a thin foil micrograph and associated set of EDS spectra, respectively, from the two phases observed in this sample at room temperature. The Widmanstätten-type microstructure is characteristic[7–12] of many austenitic and duplex ferritic/austenitic stainless steels which have experienced nonequilibrium cooling from temperatures where δ is a stable phase. The EDS spectra show that the δ phase is enriched in Cr, Mo, and Al and depleted in Ni relative to the martensite. This pattern of alloying element segregation between δ and γ (at elevated temperatures) is consistent with observations made in austenitic stainless steels by several investigators.[7–9,11–14] That δ is a stable phase in PH 13-8 Mo is not altogether surprising. Wrought 17-4 PH stainless steel can typically contain several volume percent δ, and CB-7Cu-1 and CB-7Cu-2 (cast designations of 17-4 PH and 15-5 PH, respectively) are duplex ferritic/martensitic alloys. Interpretation of microstructures evolved at 1435 °C and above is complicated by the fact that the resulting room-temperature microstructure is apparently quench-rate sensitive, as we will now describe.

Based upon the DTA and microstructural evolution presented in Figures 2 and 6, transformation to δ begins

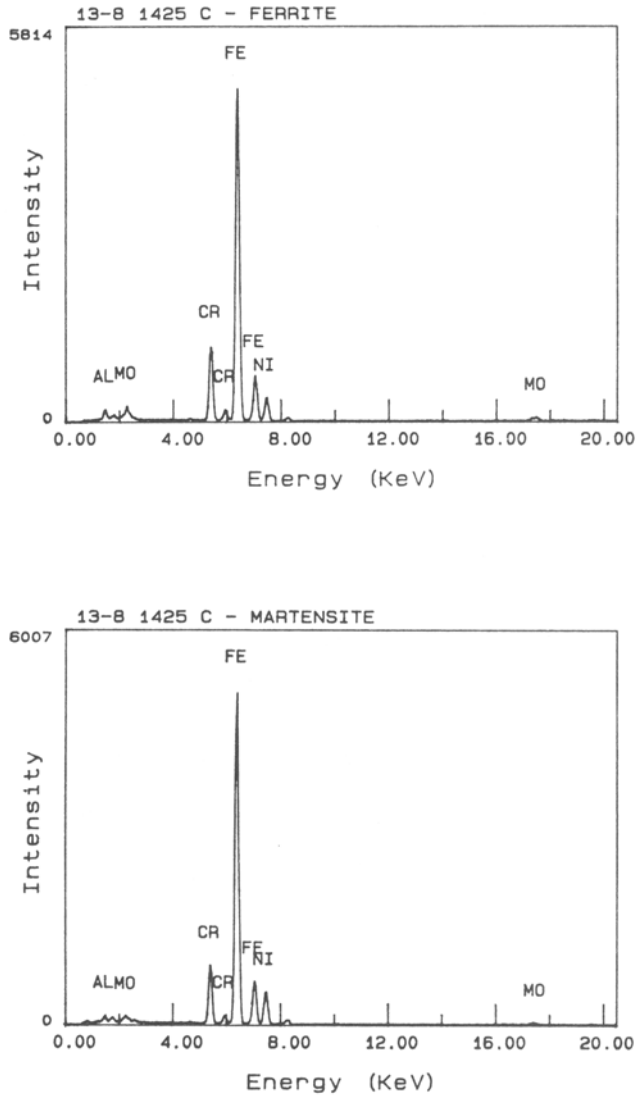

Fig. 13—EDS spectra from the δ and martensite phases shown in Figs. 6 and 12.

above 1350 °C. Cooling from the two-phase temperature range results in partial transformation of δ back to γ with the production of a Widmanstätten microstructure. Heating to temperatures of 1435 °C and above results in microstructures that are completely ferritic. Water quenching from these temperatures should result in microstructures showing evidence of a diffusional transformation characterized by the presence of a Widmanstätten microstructure. What is instead observed in the samples water quenched from both 1435 °C and 1448 °C (Figures 7 and 8) are fully martensitic grains. Martensite cannot be developed from a ferrite precursor, but instead derives from a γ parent. The lack of retained ferrite in this microstructure suggests that during the water quench, the δ grains have transformed completely to γ by a nondiffusional process. To check this hypothesis, a sample was slowly cooled (air cooled) from 1448 °C. The microstructure found in this sample is shown in Figure 14. A Widmanstätten-type microstructure, developed by a diffusion-controlled process and similar to that observed in Figure 6, is observed.

Figures 15(a) through (c) show microprobe profiles taken along the various paths defined by the microhardness indentations shown in Figures 14 and 8(b) and (c), respectively. Figure 15(a) shows the compositional variations along the path identified in Figure 14. The periodic intragranular modulation in composition (high Cr, Mo, and Al concentrations in regions of low Ni concentration) is consistent with a diffusional $\delta \Rightarrow \gamma$ transformation, resulting in the Widmanstätten $\delta + \gamma$ (martensite) microstructure.

In contrast to Figure 15(a), Figure 15(b) shows a smooth (and flat) profile within the two grains shown in Figure 8(b). A similar profile is shown in Figure 15(c), corresponding to the path indicated in Figure 8(c). A more pronounced concentration of Ni, Cr, and Mo is observed at the grain boundary in Figure 15(c) along with a distinct grain boundary structure. It is clear from the microprobe data, though, that at positions removed from grain boundaries and away from regions undergoing incipient melting that no compositional segregation consistent with

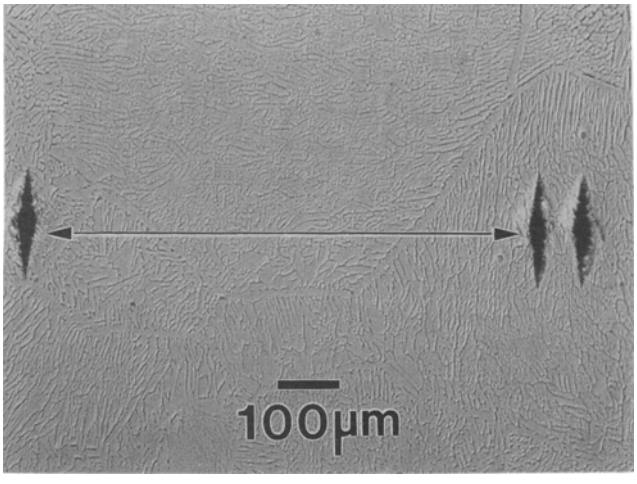

Fig. 14—Optical micrograph of sample air cooled from 1448 °C. Arrow indicates position of microprobe trace given in Fig. 15(a).

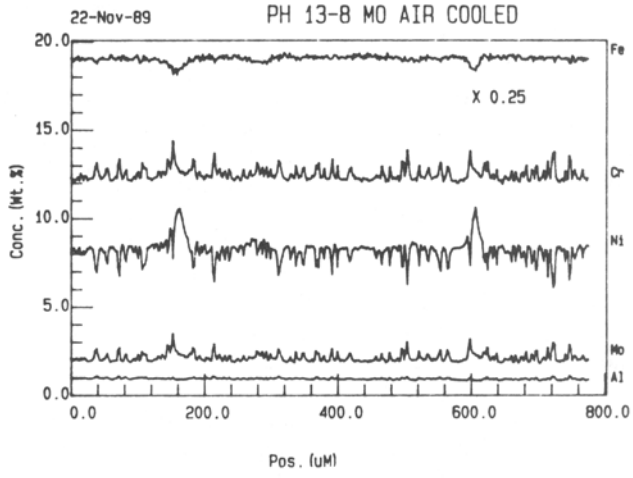

(a)

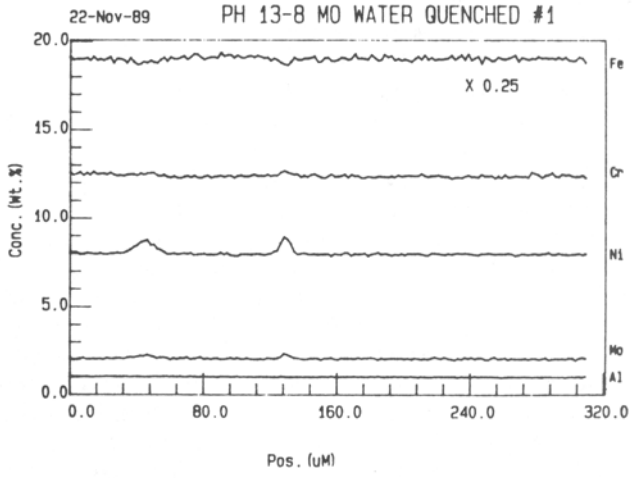

(b)

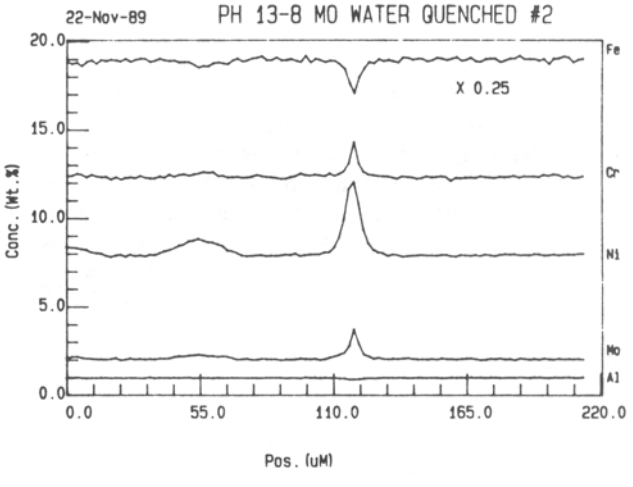

(c)

Fig. 15—Electron microprobe profiles taken across regions indicated in (*a*) Fig. 14, (*b*) Fig. 8(b), and (*c*) Fig. 8(c). JEOL Superprobe, 25 kV, 35 nA specimen current.

a diffusional transformation mechanism exists in this water-quenched sample.

The locally high Ni, Cr, and Mo concentrations at the grain boundaries in the 1448 °C WQ sample are likely related to incipient melting which occurred as the solidus was exceeded. That is, the composition of the liquid phase present at this very low volume fraction of liquid is enriched in Ni, Cr, and Mo and depleted in Fe relative to the bulk. As this sample was rapidly quenched from just above the solidus, there was no time to chemically homogenize the structure, resulting in the retention locally of a higher concentration of these alloying elements. From the compositional data, an estimate of the solidification distribution coefficients for the various alloying elements can be approximated at this very low volume fraction of liquid. The distribution coefficient is the ratio of the concentration of a particular element in the solid phase to that in the liquid phase with which it is in equilibrium. In the present case, that would be the ratio between the intragranular δ composition and the grain boundary composition. For Cr, the ratio is $\approx$0.9; for Ni, the ratio is $\approx$0.7; and for Mo, the ratio is $\approx$0.6. Note that this segregation behavior is not the same as that observed during the solid-state diffusional decomposition of $\delta \Rightarrow \gamma$ which results in δ being enriched in Cr, Mo, and Al while the γ (martensite) is enriched in Ni (Figures 4, 13, and 15(a)).

The implication of these observations is that under conditions of relatively slow cooling, nucleation and growth processes control the transformation of $\delta \Rightarrow \gamma$ in this heat of PH 13-8 Mo. Under conditions of rapid cooling where diffusional processes become suppressed and where large grains exist, limiting defect sites for nucleation, a massive transformation of $\delta \Rightarrow \gamma$ becomes operative. The thermodynamic possibility of a $\delta \Rightarrow \gamma$ massive transformation in austenitic stainless steels was first suggested by Lippold and Savage[15] who attempted to invoke this transformation process to describe the evolution of microstructure in 304/308-type austenitic stainless steel arc welds. Although it was later shown that the cooling rates associated with arc welding were too slow to result in the suppression of the diffusional transformation, subsequent investigators[12,16,17] confirmed that the formation of massive γ was possible under conditions of rapid cooling. Of particular relevance, the work of Singh *et al.*[12] established that at cooling rates as low as 100 °C/s, both grain boundary Widmanstätten γ and massive γ can exist simultaneously in an Fe-20Cr-10Ni (wt pct) alloy cooled from the single-phase δ region. At higher rates of cooling, only massive γ was observed.[12] In the present study, the lower temperature martensitic shear transformation in PH 13-8 Mo eliminates all microstructural evidence of the high-temperature $\delta \Rightarrow \gamma$ massive transformation.

Previous suggestions of Suutala *et al.*[16] that water quenching did not provide adequate cooling rates to suppress the diffusional transformation process in 304 stainless steel are not appropriate for our examination. In their study, the alloy under examination was heated only into the two-phase $\delta + \gamma$ region (1380 °C) and then subjected to either an air cool, water quench, or liquid tin quench. That is, the high-temperature microstructure was virtually identical to that established at 1425 °C (two-phase $\delta + \gamma$) in our study. With γ already present in the microstructure (as Lippold and Savage[15] had in the solidification structure of arc welds), it is very clear that extremely rapid cooling rates (liquid tin quench) would be required to suppress diffusional growth of additional γ into the thermally unstable δ because a nucleation event would not be required. In the present study, γ is not present in the microstructure at 1448 °C (or at 1435 °C), so that both a nucleation event and subsequent growth would be required to consume the high-temperature δ phase by diffusional processes.

Our microstructural observations clearly indicate that the decomposition products of δ in this heat of PH 13-8 Mo are quench-rate dependent and that the microstructural evolution can be understood simply by use of the conventional interpretation of continuous-cooling transformations. That is, a critical cooling rate exists at which diffusional processes are suppressed. At cooling rates less than this critical rate, nucleation and growth processes become operative. Mixed structures are then possible until a second (slower) critical cooling rate is reached at which the entire microstructure transforms diffusionally and no massive γ is observed. We did not quantify these critical cooling rates in the course of this work.

In summary, in the case of the PH 13-8 Mo alloy studied, the data collected are consistent with a scenario involving complete transformation of γ to δ over the temperature range $\approx$1350 °C to $\approx$1435 °C. Above $\approx$1435 °C, this alloy is completely ferritic, as the microstructures observed in Figures 7, 8, and 14 suggest. At $\approx$1447 °C, the solidus is reached (note localized areas of melting in Figure 8), as revealed by the large endotherm, and the alloy then undergoes simple single-phase melting ($\delta \Rightarrow L$) until the liquidus is reached at $\approx$1493 °C. Our interpretation of the peak of the melting endotherm being the liquidus temperature is consistent with the interpretation used by MacIssac *et al.*.[18]

B. *Solidification Behavior and Postsolidification Microstructural Development*

1. *Solidification behavior*

Analysis of the solidification behavior of this alloy can begin quite simply by examination of the microstructure observed in the DTA sample. Residual δ is observed, which is enriched in Cr, Mo, and Al and depleted in Ni relative to the martensitic matrix. Compendia of solidification microstructures of stainless steels are available[19,20,21] for comparison to the microstructures observed in PH 13-8 Mo. Consistent with the observations made in those references and with those made by investigators[22–27] studying the solidification of austenitic stainless steels, the presence of δ in the room-temperature microstructure implies a solidification sequence involving δ.

Prediction of the solidification mode of austenitic stainless steels has involved considerable research effort, primarily because of the commercial consequence of hot cracking of castings and fusion welds. Ferritic solidification has been correlated with an enhanced resistance to solidification hot cracking.[22,23,24] Because of the large number of alloying elements, both substitutional (*e.g.*, Cr, Ni, Mo) and interstitial (C, N), found in commercial alloys, statistical correlations have been used to assess

the potency of the various alloying elements in promoting ferritic *vs* austenitic solidification. The concept of the Cr and Ni equivalent compositions[25] has been developed to account for the multicomponent input to the solidification behavior of austenitic stainless steels. That is, elements, like Cr, which promote ferritic solidification (*e.g.*, Mo, Si, Ti, *etc.*) are combined together *via* appropriate weighting coefficients to arrive at an "equivalent" Cr composition, designated as Cr_{eq}. In a similar manner, elements, like Ni, which promote austenitic solidification (*e.g.*, C, N, Cu) are combined together using appropriate weighting coefficients to arrive at an equivalent Ni composition, designated as Ni_{eq}.

The most widely used equivalents for the purpose of predicting solidification mode in austenitic stainless steels are those described by Kujanpaa and Moisio,[26] as adapted from the work of Hammar and Svensson,[27] as given below.

$$Cr_{eq} = \text{wt pct Cr} + 3\ \text{wt pct Ti} + 1.5\ \text{wt pct Si} + 1.37\ \text{wt pct Mo} + 2\ \text{wt pct Nb}$$

$$Ni_{eq} = \text{wt pct Ni} + 22\ \text{wt pct C} + 14.2\ \text{wt pct N} + 0.31\ \text{wt pct Mn} + \text{wt pct Cu}$$

Applying these formulations, especially the Cr_{eq}, to calculate equivalent chemistries for alloy PH 13-8 Mo would be difficult, as Al does not appear as an alloying element in either equivalent formulation. In his work on the formation of martensite in stainless steels, Hull[28] ascribed a weighting factor of 2.48 for Al in his Cr_{eq} formulation. Although Hull's work was not aimed at predicting solidification mode, the potency of Al as a ferrite stabilizer was established. Other investigators[29,30,31] have also recognized the ferrite stabilizing influence of Al with weighting factors as high as 4 being established. Applying the equivalent relationships developed from studies of austenitic stainless steels to predict solidification behavior for the PH steels should be reasonably valid because the same high-temperature phases exist in each class of alloys.

Using the Hammar and Svensson[27] equivalent relationships, a Cr_{eq} of 18.46 (when 2.48 wt pct Al is added) and a Ni_{eq} of 8.69 can be calculated for the heat of PH 13-8 Mo under study. Kujanpaa and Moisio[26] predict primary δ solidification (with γ solidification terminating freezing) will occur when the ratio $Cr_{eq}/Ni_{eq} > 1.5$. When this ratio rises in value to >2.0, solidification completely to δ is predicted. For the PH 13-8 Mo alloy examined, a Cr_{eq}/Ni_{eq} of 2.12 is obtained (when 2.48 wt pct Al is added), which predicts fully ferritic solidification (primary δ followed by terminal γ is predicted if the Al contribution is not added) for this alloy.

2. *Postsolidification microstructural development*

In the case of the alloy presently under discussion, the on-cooling portion of the DTA thermogram is interpreted to describe solidification as δ, with subsequent solid-state transformation to γ beginning at ≈1364 °C. That is, the following reaction path is proposed:

$$L \Rightarrow L + \delta \Rightarrow \delta \Rightarrow \delta + \gamma$$

For this interpretation to be accurate, three microstructural observations are required. First, there must be clear evidence of ferritic solidification. Second, there must be no evidence of a liquid phase remaining at temperatures between 1411 °C and 1364 °C (otherwise, the exothermic reaction beginning at ≈1364 °C could be indicating a terminal solidification event involving γ). Third, the completion of the exothermic reaction beginning at 1364 °C should reveal a phase transformed microstructure similar to that observed in the DTA sample (confirming that this event represents the $\delta \Rightarrow \gamma$ transformation).

Figure 9(a) shows the microstructure obtained from the sample quenched from 1450 °C. Within the coarse cellular structure is the Widmanstätten substructure which occurs when high-temperature δ transforms to γ on quenching, as described above. This observation confirms solidification as δ and is consistent with a complete transformation of γ to δ on heating before the solidus is reached. That the diffusional (in lieu of the massive) transformation of δ to γ occurs within this structure requires comment. Although the large solidification cells are clearly ferritic, these samples were quenched while a substantial amount of the structure was still liquid. Dissipation of the latent heat of fusion during the quenching operation would clearly lower the effective cooling rate, possibly into the range where the diffusional mechanisms were operative. In addition, the morphology of the solidification structure itself would result in the presence of additional defect sites for subsequent nucleation of the solid-state transformation. The composition of the δ itself is not the same as that examined in Figure 8, as this δ is quenched from a two-phase $L + \delta$ region. Finally, the quenching operation itself may have an influence. This could occur in two ways. First, some systematic variation in quench rate is likely from sample to sample. A second more subtle possibility is that as the remaining liquid solidifies, now under extremely nonequilibrium conditions, terminal solidification to γ cannot be ruled out.[32] If γ were to form as a terminal solidification constituent under these conditions, then growth of γ into thermally unstable δ upon cooling would be simple.

Figure 10 shows the microstructure obtained on quenching the alloy from 1375 °C. No residual liquid phase (as would be evidenced by the presence of a fine solidification substructure) was observed. Rather, a very coarse duplex microstructure is evident with no remnant solidification substructure. The absence of solidification substructure is further evidence that solidification proceeded to completion as δ. The body-centered-cubic crystal structure of δ phase promotes relatively rapid diffusion rates in comparison to the face-centered-cubic γ structure.[33] Chemical homogenization is, therefore, more likely in a completely ferritic structure, resulting in the effective elimination of the original cellular solidification microstructure.[11] The duplex microstructure consisting of a coarse Widmanstätten constituent and large areas of single-phase martensite suggests that transformation from δ to γ involved both massive and diffusional processes, similar to that observed by Singh *et al.*[12]

From the data obtained during the on-heating portion of the thermal cycle, it is clear that both γ and δ are equilibrium phases at temperatures between ≈1350 °C

and ≈1435 °C. Under truly equilibrium cooling conditions, then, it would be anticipated that γ would appear in the microstructure at a temperature of ≈1435 °C and continue to grow at the expense of the δ phase until δ was exhausted at ≈1350 °C. Reviewing the microstructure of the DTA sample (Figure 3), it is obvious that equilibrium is not achieved at cooling rates of 0.33 °C/s because residual δ is present in the microstructure of this sample. Nonequilibrium transformations on cooling generally result in undercooling of the parent phase (δ) prior to nucleation of the daughter phase (γ). In a study of the $\delta \Rightarrow \gamma$ transformation in duplex stainless steels, Mundt and Hoffmeister[34] reported undercoolings as large as 100 °C at cooling rates comparable to those used in this study. If γ were present at temperatures above 1364 °C (at the examined cooling rate), such as at the termination of solidification, it would be expected that a continuous transformation of δ to γ would be occurring and that the heat of transformation would be evidenced on the DTA thermogram at temperatures above 1364 °C. That it is not implies that the exothermic reaction initiating at ≈1364 °C must represent the nucleation temperature of γ during continuous cooling of PH 13-8 Mo at the rate of 0.33 °C/s, supporting the postulate that γ does not appear as a solidification phase under these experimental conditions.

Figure 11 shows the microstructure obtained upon quenching from 1300 °C. Again, no evidence of a solidification event remains in this sample except for the presence of shrinkage porosity (not shown in this section). Instead, a two-phase microstructure is present in which the minor phase is featureless and the matrix has a lath substructure. The similarity in microstructures observed in the DTA sample (Figure 3) and the sample quenched from 1300 °C strongly suggests that very little microstructural modification occurs in this alloy below 1300 °C at the cooling rate examined.

All of the microstructural observations required to prove the proposed transformation sequence given above have thus been made. Using Hull's weighting factor for Al[28] in the Hammar and Svensson[27] Cr_{eq} formulation, complete ferritic solidification is predicted (and observed experimentally) using the criterion of Kujanpaa and Moisio.[26]

The presence of residual δ indicates that insufficient time was available at the cooling rate examined to allow the $\delta \Rightarrow \gamma$ transformation to go to completion. A similar situation occurs in many austenitic stainless steels, resulting in a duplex microstructure in which the residual ferrite is enriched in ferrite stabilizing elements, such as Cr and Mo, and depleted in Ni.[13]

C. *Implications*

An implication of these observations is that residual δ may be observable in fusion welds and castings of PH 13-8 Mo. Figure 16 is an optical micrograph of an autogenous (no filler metal added) gas-tungsten-arc (GTA) weld made on the same heat of PH 13-8 Mo used in this study. A two-phase (martensite + δ) microstructure is seen. Microstructures of this type have been shown to be optimal relative to the weldability (resistance to hot cracking) of austenitic stainless steels. Indeed, in a related study,[35] the hot cracking resistance of this heat of PH 13-8 Mo was shown to be comparable to 304L stainless steel. Similar results have been reported previously by Cieslak *et al.*[3] Figure 17 is an optical micrograph showing the as-cast microstructure of a PH 13-8 Mo investment casting (Fe-12.4Cr-8.1Ni-2.2Mo-0.8Al-0.04C-0.04Si wt pct). A small amount of residual δ in a martensitic matrix is again observed. Elmer[17] recently performed a first-order analysis of the effects of solidification and cooling rates on the volume fraction of δ retained in the solidification structure of Fe-Cr-Ni ternary stainless steels. He concluded that lower solidification and cooling rates will result in a smaller amount of retained δ, even though the solidification structure (and, hence, diffusion length) is coarser. From this analysis, it can be inferred that larger castings of certain chemistries of PH 13-8 Mo may be nearly δ free in comparison to more rapidly solidified structures.

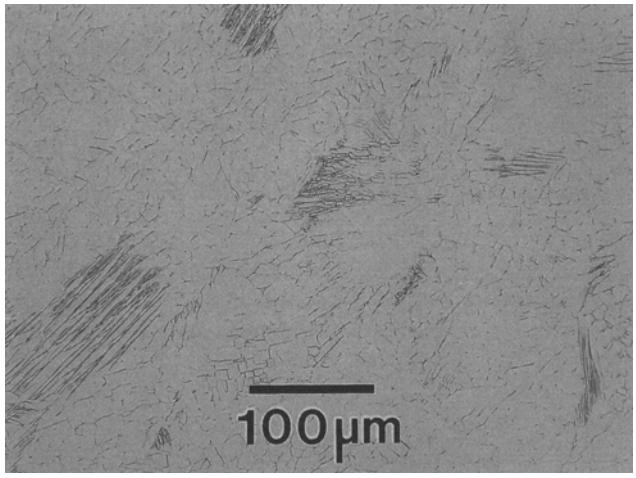

Fig. 16—Microstructure of as-GTA welded PH 13-8 Mo (100 amps, electrode negative; 3.3 mm/s travel speed).

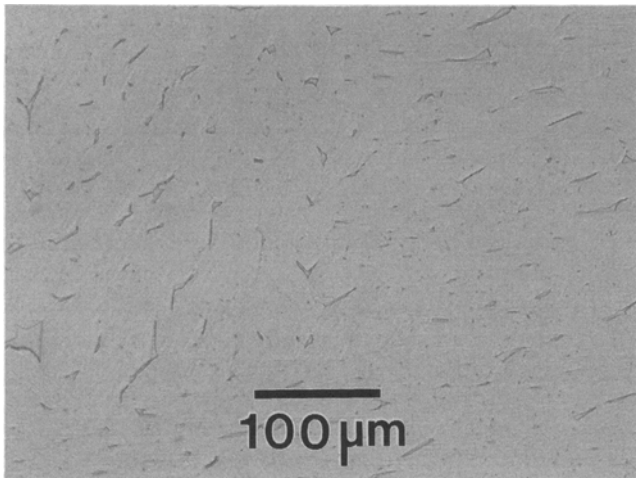

Fig. 17—As-solidified microstructure of investment cast PH 13-8 Mo.

V. CONCLUSIONS

For the heat of PH 13-8 Mo examined, the following conclusions apply. Transformation of γ to δ occurs on heating, beginning at a temperature of $\approx$1350 °C and concluding by a temperature of $\approx$1435 °C. The alloy solidus is $\approx$1447 °C and the alloy liquidus is $\approx$1493 °C. At a cooling rate of 0.33 °C/s, the alloy solidifies completely to δ with solid-state transformation of δ to γ beginning at $\approx$1364 °C, resulting in Widmanstätten γ formation with residual δ. The residual δ is enriched in Cr, Mo, and Al and depleted in Ni relative to the matrix martensite (prior γ). The $\delta \Rightarrow \gamma$ transformation process is quench-rate sensitive. Fully ferritic structures can transform to γ massively or *via* a diffusional process, depending upon the cooling rate. Using Hull's weighting factor (2.48) for the contribution of Al to the Cr_{eq} defined by Hammar and Svensson results in a prediction of fully ferritic solidification (as is observed) using the criterion of Kujanpaa and Moisio. Residual δ is observed in gas-tungsten-arc fusion welds made on this alloy. The as-solidified microstructure observed in a typical investment casting of PH 13-8 Mo is duplex δ + martensite.

ACKNOWLEDGMENTS

The authors would like to thank Bill Swartout for performing the DTA experiments and Ellen Semarge, Alice Kilgo, and Tom Lienert for microprobe, metallographic, and laboratory assistance, respectively. This work was performed at Sandia National Laboratories, supported by the United States Department of Energy under Contract No. DE-AC04-76DP00789, and at Oak Ridge National Laboratory, operated by Martin Marietta Energy Systems, Inc., under Contract No. DE-AC05-840R21400 with the United States Department of Energy.

REFERENCES

1. *Aerospace Structural Metals Handbook*, Belfour Stulen, Inc., Traverse City, MI, 1974, no. 2, code 1510, pp. 1-19.
2. E.L. AuBuchon and R.V. London: *Met. Prog.*, May 1981, pp. 35-37.
3. W.R. Cieslak, J.A. Brooks, and W.M. Garrison, Jr.: in *Advances in Welding Science and Technology*, S.A. David, ed., ASM, Metals Park, OH, 1986, pp. 515-22.
4. M.J. Cieslak: *Weld. J.*, 1987, vol. 66, pp. 57s-60s.
5. M.J. Cieslak and S.A. David: *Abstracts of Papers—69th American Welding Society Annual Meeting*, Washington, DC, Apr. 17–22, 1988, American Welding Society, Miami, FL, pp. 74-77.
6. W.F. Chambers: *Sandia TASK8: A Subroutined Electron Microprobe Automation System*, Sandia Report No. SAND85-2037, Sandia National Laboratories, Albuquerque, NM, 1985.
7. N. Suutala, T. Takalo, and T. Moisio: *Metall. Trans. A*, 1980, vol. 11A, pp. 717-25.
8. M.J. Cieslak and W.F. Savage: *Weld. J.*, 1980, vol. 59, pp. 136s-146s.
9. J.C. Lippold and W.F. Savage: *Weld. J.*, 1980, vol. 59, pp. 48s-58s.
10. S.A. David: *Weld. J.*, 1981, vol. 60, pp. 63s-71s.
11. G.L. Leone and H.W. Kerr: *Weld. J.*, 1982, vol. 61, pp. 13s-22s.
12. J. Singh, G.R. Purdy, and G.C. Weatherly: *Metall. Trans. A*, 1985, vol. 16A, pp. 1363-69.
13. M.J. Cieslak, A.M. Ritter, and W.F. Savage: *Weld. J.*, 1982, vol. 61, pp. 1s-8s.
14. Ann M. Ritter, Michael F. Henry, and Warren F. Savage: *Metall. Trans. A*, 1984, vol. 15A, pp. 1339-51.
15. J.C. Lippold and W.F. Savage: *Weld. J.*, 1979, vol. 58, pp. 362s-374s.
16. N. Suutala, T. Takalo, and T. Moisio: *Weld. J.*, 1981, vol. 60, pp. 92s-93s.
17. John Walter Elmer: *The Influence of Cooling Rate on the Microstructure of Stainless Steel Alloys*, Lawrence Livermore National Laboratory Document UCRL-53934, Livermore, CA, Sept. 1988.
18. D.G. MacIssac, Y. Shiohara, M.G. Chu, and M.C. Flemings: in *Grain Refinement in Castings and Welds*, G.J. Abbaschian and S.A. David, eds., TMS, Warrendale, PA, 1983, pp. 87-96.
19. *A Guide to the Solidification of Steels*, Jernkontoret, Stockholm, Sweden, 1977.
20. *Metals Handbook*, 8th ed., ASM, Metals Park, OH, 1972, vol. 7, pp. 152-56.
21. *Microstructures of Heat-Resistant Alloys*, Alloy Casting Institute Division of Steel Founders' Society of America, Des Plaines, IL, 1970.
22. F.C. Hull: *Weld. J.*, 1967, vol. 46, pp. 399s-409s.
23. Y. Arata, F. Matsuda, and S. Katayama: *Trans. Jpn. Weld. Res. Inst.*, 1977, no. 6, pp. 105-16.
24. J.C. Lippold and W.F. Savage: *Weld. J.*, 1982, vol. 61, pp. 388s-396s.
25. A.L. Schaeffler: *Met. Prog.*, 1949, vol. 56, pp. 680-680b.
26. V. Kujanpaa and T. Moisio: in *Solidification Technology in the Foundry and Casthouse*, The Metals Society, London, 1980, session IVb, pp. 1-8.
27. O. Hammar and U. Svensson: in *Solidification and Casting of Metals*, The Metals Society, London, 1979, pp. 401-10.
28. F.C. Hull: *Weld. J.*, 1973, vol. 52, pp. 193s-203s.
29. K.J. Irvine, D.T. Llewellyn, and F.B. Pickering: *J. Iron Steel Inst.*, July 1959, pp. 218-38.
30. M. Potak and E.A. Sagalevich: *Avtom Svarka*, May 1972, pp. 10-13.
31. P. Guiraldenq: *Rev. Metall.*, 1967, vol. 64, pp. 907-39.
32. N. Suutala: *Metall. Trans. A*, 1983, vol. 14A, pp. 191-97.
33. Erich Folkhard: in *Welding Metallurgy of Stainless Steels*, Springer-Verlag, New York, NY, 1988, p. 50.
34. R. Mundt and H. Hoffmeister: *Arch. Eisenhuettenwes.*, 1983, vol. 54, pp. 333-36.
35. M.J. Cieslak: Sandia National Laboratories, Albuquerque, NM, unpublished research, 1988.